Analysis and Computation for a Fluid Mixture Model

Qunlei Jiang, Zhilin Li* and Sharon R. Lubkin

Department of Mathematics & Center for Scientific Computations, North Carolina State University, Raleigh, NC 27695, USA.

Abstract. A fluid mixture model of tissue deformations has been studied in this paper. The model is a mixed system of nonlinear hyperbolic and elliptic partial differential equations. Both theoretical linear stability and numerical analysis are presented. Comparisons between standard numerical methods that utilize Runge-Kutta methods coupled with the WENO scheme and the immersed interface methods are given. Numerical examples are also presented.

AMS subject classifications: 65N06, 65N12, 65M06, 76M20

Key words: Tissue deformations, immersed interface method, linear stability analysis, finite difference method.

1 Introduction

In this paper, we consider a mathematical model developed in [3,8,9] for modeling deformations of contractile mesenchymal tissues. The tissues are considered to be composed of two inter-penetrating material phases: an aqueous phase and a cell-fiber phase. The aqueous phase is composed of all the water and dissolved extracellular components of the tissues. The cell-fiber phase consists of the cells and the remaining, generally fibrous, extracellular components. It is assumed that: (1) the two phases occupy complementary portions of the space, (2) the aqueous phase behaves as a Stokes fluid, (3) the stresses in the cell-fiber phase are dissipated by permanent deformation on the relevant time scale and can also be treated as a Stokes flow. These assumptions lead to the following system

---

*Corresponding author. *Email addresses:* `qjiang2@gmail.com` (Q. Jiang), `zhilin@math.ncsu.edu` (Z. Li), `lubkin@math.ncsu.edu` (S. R. Lubkin)

of partial differential equations (in 1D):

$$\frac{\partial \theta}{\partial t} + \frac{\partial (\theta v)}{\partial x} = 0, \quad 0 < x < L, \tag{1.1}$$

$$\frac{\partial}{\partial x} \left(\frac{1-\theta}{\varphi \theta} \cdot \frac{\partial p}{\partial x} - v \right) = 0, \tag{1.2}$$

$$\frac{\partial}{\partial x} \left(2M \frac{\partial v}{\partial x} - p + \theta \psi + \sigma \ln(1-\theta) \right) = 0, \tag{1.3}$$

where $0 < \theta < 1$ is the volume fraction of cells and fibers, v is the velocity of the cell-fiber phase, p is the pressure, φ is the drag coefficient, ψ is the contractility coefficient, σ is the swelling coefficient, and M is the viscosity coefficient of the cell-fiber fraction. Note that the parameters φ, M, ψ and σ are nonnegative and can depend on time, space, and θ.

A reasonable range of dimensional and non-dimensional parameters are presented in Table 1; see [3, 8] for the references.

Table 1: Expected ranges of parameter values in which ϵ is a small positive number.

parameter	symbol	units	range
specific drag coefficient	φ	kg/m^3-sec	$10^{12} \sim 10^{14}$
tissue viscosity	M	kg/m-sec	10^5
specific contractility coefficient	ψ	kg/m-sec^2	$10^3 \sim 10^4$
swelling number	σ	kg/m-sec^2	$10 \sim 10^3$
volume fraction of cell-fiber phase	θ_0	-	$\epsilon \sim (1-\epsilon)$

The boundary conditions (BC) are given as follows

$$v(0,t) = v(L,t) = 0, \quad \frac{\partial \theta}{\partial x}(0,t) = \frac{\partial \theta}{\partial x}(L,t) = 0, \quad \frac{\partial p}{\partial x}(0,t) = \frac{\partial p}{\partial x}(L,t) = 0. \tag{1.4}$$

One way to model two adjacent tissues is to simply include them in the same equations and account for their different densities with θ. Thus a simple interaction between two tissues can be modeled with piecewise constant initial condition (see Fig. 1),

$$\theta(x,0) = \begin{cases} \theta_l, & \text{if } 0 \leq x < x_1 \text{ or } x_2 < x \leq L, \\ \theta_u, & \text{if } x_1 \leq x \leq x_2, \end{cases} \tag{1.5}$$

where we use θ_l for the smaller constant (lower), and θ_u for the larger constant (upper).

In this paper, we will focus on simulating tissue deformations numerically for the one dimensional model. Note that the mathematical model is a non-linear, mixed (hyperbolic and elliptic) system of differential equations. Shock waves will be developed in
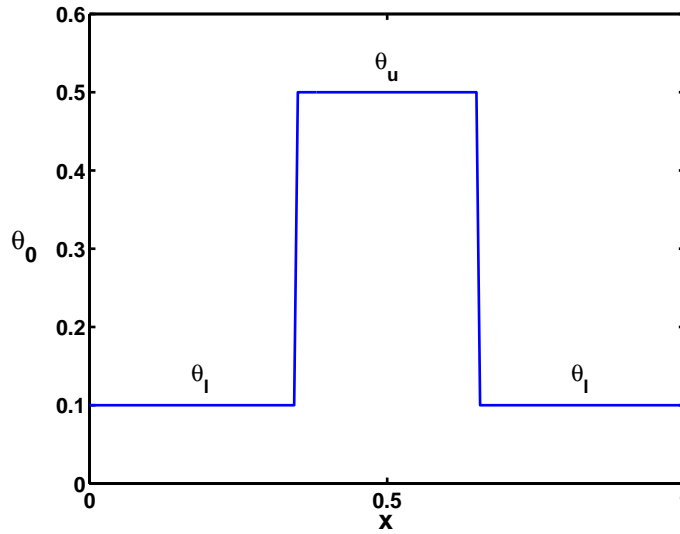
Figure 1: A typical initial data of θ.

the time evolution process. The purpose of this paper is to investigate the stability of the equilibria, and to verify stability and accuracy of our numerical methods.

We will present two numerical methods to solve the one-dimensional system. The first one is to use high order numerical methods such as WENO (weighted essentially non-oscillatory) schemes, for example, [2,4,10] for the hyperbolic equation and the standard central finite difference scheme for the elliptic equation. In the second approach, we use the immersed interface method to track the shock waves, which avoids non-physical oscillations.

2 The linear stability analysis

There are four physical coefficients, φ, M, ψ and σ in the system (1.1)-(1.3). In order to predict the overall behavior of the solution, it is necessary to carry out linear stability analysis.

An obvious steady state of the model, which can be easily verified, is the following

$$\begin{bmatrix} \theta \\ v \\ p \end{bmatrix} = \begin{bmatrix} \theta_0 \\ v_0 \\ p_0 \end{bmatrix}, \tag{2.1}$$

where θ_0 is a constant. For simplicity, we will take $v_0 = p_0 = 0$. We have the following theorem about the stability of the equilibrium.

Theorem 2.1. *Assume that the parameters φ, M, ψ and σ in (1.1)-(1.3) only depend on θ. Then*

the solution (2.1) *of the system* (1.1)-(1.3) *is unstable if*

$$\psi + \frac{\partial \psi}{\partial \theta}\theta + \frac{\partial \sigma}{\partial \theta}\ln(1-\theta) > \frac{\sigma}{1-\theta}, \tag{2.2}$$

where the functions ψ, σ, *and their derivatives are evaluated at* θ_0. *Otherwise it is stable.*

Sketch of the proof. We consider small perturbations of the form

$$\begin{bmatrix} \theta \\ v \\ p \end{bmatrix} = \begin{bmatrix} \theta_0 \\ 0 \\ 0 \end{bmatrix} + \varepsilon \begin{bmatrix} \theta_1 \\ v_1 \\ p_1 \end{bmatrix} = \begin{bmatrix} \theta_0 \\ 0 \\ 0 \end{bmatrix} + \varepsilon \begin{bmatrix} c_1 \\ c_2 \\ c_3 \end{bmatrix} e^{\lambda t + ikx}, \quad 0 < \varepsilon \ll 1, \tag{2.3}$$

where c_1, c_2 and c_3 are constants and k is a typical Fourier mode.

Plugging in θ, v, and p above into (1.1)-(1.3), expanding all terms using the Taylor expansion, and collecting the terms corresponding to ε, we get

$$\lambda = \frac{k^2 \frac{1-\theta_0}{\varphi_0}\left(\psi_0 + (\psi_0)'_\theta \theta_0 + (\sigma_0)'_\theta \ln(1-\theta_0) - \frac{\sigma_0}{1-\theta_0}\right)}{1 + 2k^2 M_0 \frac{1-\theta_0}{\varphi_0 \theta_0}}, \tag{2.4}$$

where

$$\varphi_0 = \varphi(\theta_0), \quad \psi_0 = \psi(\theta_0), \quad \sigma_0 = \sigma(\theta_0), \quad M_0 = M(\theta_0),$$

$$(\psi_0)'_\theta = \frac{\partial \psi}{\partial \theta}(\theta_0), \quad (\sigma_0)'_\theta = \frac{\partial \sigma}{\partial \theta}(\theta_0).$$

Note that λ is a function of k^2, and it is a real number and bounded. The system is unstable if $\lambda > 0$, which is true when

$$\psi_0 + (\psi_0)'_\theta \theta_0 + (\sigma_0)'_\theta \ln(1-\theta_0) - \frac{\sigma_0}{1-\theta_0} > 0. \tag{2.5}$$

To analyze the system further, we need to choose specific ψ and σ. To facilitate testing our method on various functional forms, we nondimensionalized the system using length scale L of 1 mm and time scale 1 hour. We analyzed and simulated several cases listed in Table 2.

Table 2: Choices of the nondimensionalized functions φ, ψ, and σ. In the table ϵ is a small positive number.

Models	M	φ	ψ	σ
1	0.5	ϵ	C_1	C_2
2	$\frac{\theta}{0.5+\theta}$	1.0	θ	$1-\theta$
3	$0.5e^\theta$	e^θ	C_1	C_2
4	$0.5e^\theta$	e^θ	$1.8e^{-\theta}$	$e^{-\theta}$

Note that the stability condition (2.5) depends on θ_0, ψ, σ, and derivatives of ψ and σ. Hence we can treat Models 1 and 3 in the same way since in both cases ψ and σ are constants. In these two cases, λ can be expressed as

$$\lambda = \frac{k^2 \frac{1-\theta_0}{\varphi_0}\left(\psi_0 - \frac{\sigma_0}{1-\theta_0}\right)}{1+2k^2 M_0 \frac{1-\theta_0}{\varphi_0 \theta_0}}. \tag{2.6}$$

The system is unstable for all k if (2.5), which is reduced to

$$\psi_0 > \frac{\sigma_0}{1-\theta_0},$$

that is, when contractility outweighs swelling, instability results.

We are also interested in the case where the initial θ has a jump discontinuity as plotted in Fig. 1, in which we take $L=1$ for simplicity of the discussion and thereafter. In general, the tissue will swell or contract to an equilibrium state. For such an initial θ, we can determine ψ that makes the system be an equilibrium state. Note that $\partial \theta / \partial t = 0$ but θ_x does not exist at the discontinuities. We use

$$[\theta] = \lim_{x \to \alpha^+} \theta(x) - \lim_{x \to \alpha^-} \theta(x) = \theta^+ - \theta^-$$

to denote the jump of θ at $x=\alpha$. For Model 1, it is easy to get the relation of the parameters in the equilibrium,

$$-\psi[\theta] - \sigma[\ln(1-\theta)] = 0. \tag{2.7}$$

Hence,

$$\psi = -\frac{\sigma[\ln(1-\theta)]}{[\theta]} = -\frac{\sigma(\ln(1-\theta_u) - \ln(1-\theta_l))}{\theta_u - \theta_l}. \tag{2.8}$$

For the other models, it is much more complicated to find such relation of the parameters corresponding to equilibrium state.

When $\psi = \sigma / (1-\theta_0)$, we conclude that $\lambda = 0$ indicating a neutral stability. Fig. 2 shows the plot of the values ψ determined by (2.8), $\psi(\theta_l) = \sigma / (1-\theta_l)$, and $\psi(\theta_u) = \sigma / (1-\theta_u)$ with $\sigma = 1$, and $\theta_l = 0.1$. Fig. 2 indicates that for the given σ and θ_l, the system will be at the steady state if one chooses ψ and θ_u along the solid curve; the system will be stable if one chooses ψ under the dash-dot horizontal line; the system will be unstable if one chooses ψ above the dashed curve; and the system will be unsettled with the solution near θ_l appearing to be unstable and the solution near θ_u appearing to be stable if one chooses ψ and θ_u from the region under the dashed curve and above the dash-dot horizontal line. We will call this region an oscillation region. Note that the steady state curve always lies between $\psi(\theta_l)$ and $\psi(\theta_u)$. This implies that any perturbation around the steady state with the piecewise constant initial θ will be depressed at the middle part (the solution near θ_u) but the solution will grow near the two ends (the solution near θ_l).
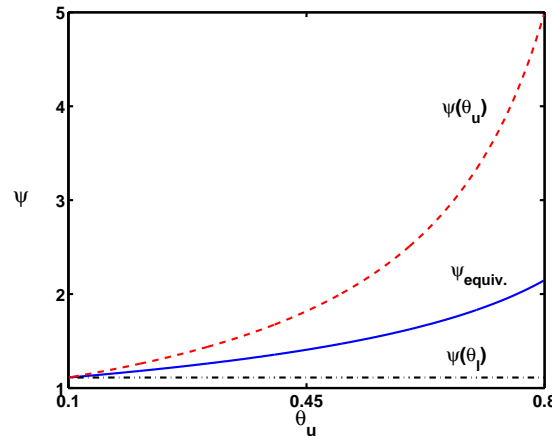
Figure 2: The plot of stability region of system with $\sigma=1$, $\psi=\frac{\sigma}{1-\theta}$, $\psi_{equiv.}$ determined by (2.8), and $\theta_l=0.1$. The dashed line and dash-dot line indicate the ψ with which the system is neutral stable for θ_u and θ_l, respectively; the solid line indicates the ψ value with which the system is at equilibrium.

We demonstrate the stability analysis in Fig. 3 with the initial condition

$$\theta(x,0)=\begin{cases} \theta_l+\varepsilon\cos(kx), & \text{if } 0\leq x<x_1 \text{ or } x_2<x\leq 1, \\ \theta_u+\varepsilon\cos(kx), & \text{if } x_1\leq x\leq x_2. \end{cases} \tag{2.9}$$

The parameters are $\sigma=1.0$, $\theta_u=0.5$, $\theta_l=0.1$, $\psi=1.47$, $\varepsilon=0.05$, $k=60\pi$, $x_1=0.4$, and $x_2=0.6$.

In Fig. 3, the dash-dot line in the plot shows the steady state solution; the dotted line shows the initial data and the solid line shows the solution at $t=20$. As discussed above, the perturbation middle part decays in time and approaches steady state, and the perturbation near the two ends grows with time.

For Model 2 and 4, we still can find the eigenvalue relations for the stability analysis, but it is difficult to find the exact steady state solutions in terms of the parameters.

The parameters for Model 2 are

$$\psi=\theta, \quad \sigma=1-\theta. \tag{2.10}$$

We have derived that

$$\lambda=\frac{k^2\frac{1-\theta_0}{\varphi_0}(2\theta_0-\ln(1-\theta_0)-1)}{1+2k^2M_0\frac{1-\theta_0}{\varphi_0\theta_0}}. \tag{2.11}$$

The system is unstable if (2.5), which is reduced to

$$2\theta_0-\ln(1-\theta_0)-1>0$$

in this case. Using the MATLAB built-in function *fzero*, it is easy to find that $\lambda>0$ when $\theta_0>0.31$.

(a) Solution for θ (b) Solution for v
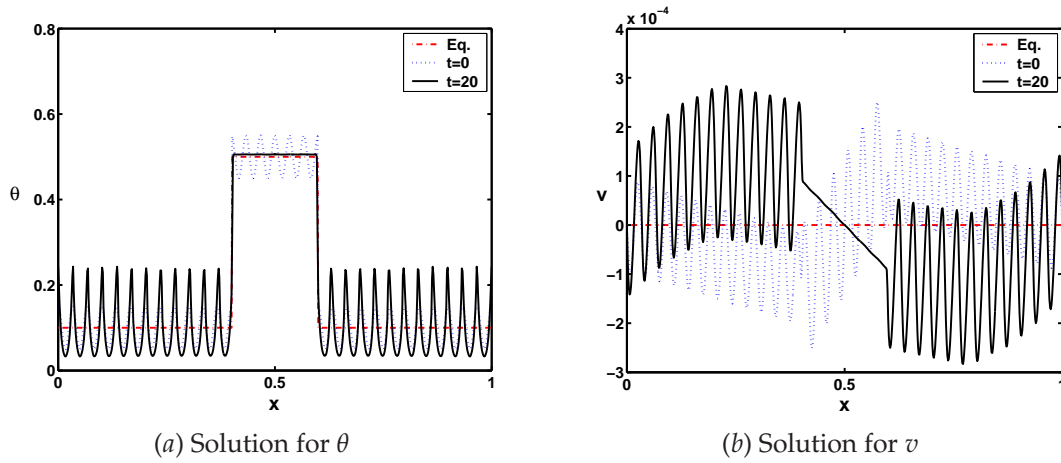
Figure 3: Solution plots with the perturbed initial data (2.9) with $M=0.5$, $\varphi=0$, $\sigma=1$, $\psi=1.47$, $\theta_u=0.5$, $\theta_l=0.1$, $\varepsilon=0.05$, $k=60\pi$, $x_1=0.4$, and $x_2=0.6$. In both plots, the dash-dot line shows the steady state; the dotted one shows the initial data and the solid one shows the solution at $t=20$.

The parameters for Model 4 are

$$M=0.5e^{\theta}; \quad \varphi=e^{\theta}; \quad \psi=1.8e^{-\theta}; \quad \sigma=e^{-\theta}. \tag{2.12}$$

We have showed that λ can be expressed as

$$\lambda=\frac{k^2\theta_0(1-\theta_0)e^{-2\theta_0}f(\theta_0)}{\theta_0+k^2(1-\theta_0)}, \tag{2.13}$$

where

$$f(\theta_0)=1.8(1-\theta_0)-\ln(1-\theta_0)-\frac{1}{1-\theta_0}. \tag{2.14}$$

Note that the sign of λ depends on the sign of $f(\theta_0)$. Hence, the system is unstable under (2.5), which is reduced to

$$1.8(1-\theta_0)-\ln(1-\theta_0)-\frac{1}{1-\theta_0}>0.$$

For smaller θ, say, $\theta<0.37$, we have $\lambda>0$, and the linearized system is unstable. For larger θ, we have $\lambda<0$, and the linearized system is stable and will approach the equilibrium. For the piecewise constant initial condition with $\theta_l<0.37$ and $\theta_u>0.37$, the situation is the same as in Model 1 and 3. The solution is unstable near the ends but stable in the middle. This presents a challenge for numerical computations.

3 Numerical methods

From (1.2), one can obtain

$$\frac{1-\theta}{\varphi\theta}p_x-v=c,$$

where c is a constant. Applying the boundary conditions for pressure and velocity, we have $c=0$, i.e., $(1-\theta)p_x/(\varphi\theta)=v$. We can eliminate p from the system (1.1)-(1.3) to get

$$\frac{\partial\theta}{\partial t}+\frac{\partial(\theta v)}{\partial x}=0, \tag{3.1}$$

$$\frac{\partial}{\partial x}\left(2M\frac{\partial v}{\partial x}\right)-\frac{\varphi\theta}{1-\theta}v+\frac{\partial(\theta\psi)}{\partial x}+\frac{\partial(\sigma\ln(1-\theta))}{\partial x}=0. \tag{3.2}$$

Our numerical computation is based on the above simplified system. Finite difference methods are employed to solve the system. A Runge-Kutta method is used for time discretization. The WENO scheme is used for spatial discretization for the hyperbolic equation. We describe two approaches. The first approach assumes no knowledge of the shock locations. The second approach is the immersed interface method that uses the jump conditions to solve the differential equations to second order accuracy assuming knowledge of the locations of the discontinuities.

3.1   The WENO-Roe scheme

For the hyperbolic equation (3.1), we use the fifth order WENO scheme with Roe flux (WENO-Roe) for the spatial discretization, combined with third order TVD (total variation diminishing) Runge-Kutta method [1,2,4,10] for the time discretization.

We use a uniform grid

$$a=x_0<x_1<\cdots<x_{N-1}<x_N=L \tag{3.3}$$

and define

$$x_{i+\frac{1}{2}}=\frac{x_i+x_{i+1}}{2}, \quad i=0,1,\cdots,N-1. \tag{3.4}$$

The conservative approximation to the spatial derivative is applied directly to (3.1)

$$\frac{d\theta_i(t)}{dt}=-\frac{1}{\Delta x}(\hat{f}_{i+\frac{1}{2}}-\hat{f}_{i-\frac{1}{2}}), \tag{3.5}$$

where $\theta_i(t)$ is the numerical approximation to $\theta(x_i,t)$, and $\hat{f}_{i+\frac{1}{2}}$ is the numerical flux. Let $u(x)=f(\theta(x,t))=\theta v$. Let the finite difference stencils be

$$S_r(i)=\{x_{i-r},\cdots,x_{i-r+k-1}\}, \quad r=0,\cdots,k-1. \tag{3.6}$$

We can get $2k$ different ENO reconstructions to form the upwind biased kth order approximations to the values $u_{i+\frac{1}{2}}^{(r)}$ and $u_{i-\frac{1}{2}}^{(r)}$, that is,

$$u_{i+\frac{1}{2}}^{(r)}=\sum_{j=0}^{k-1}c_{rj}u_{i-r+j}, \quad u_{i-\frac{1}{2}}^{(r)}=\sum_{j=0}^{k-1}\tilde{c}_{rj}u_{i-r+j}, \quad r=0,\cdots,k-1. \tag{3.7}$$

Note that $\tilde{c}_{rj} = c_{r-1,j}$, where

$$c_{rj} = \sum_{m=j+1}^{k} \frac{\sum_{l=0,l\neq m}^{k} \prod_{q=0,q\neq m,l}^{k} (r-q+l)}{\prod_{l=0,l\neq m}^{k} (m-l)} \qquad (3.8)$$

for a uniform grid. We list the constants c_{rj} for $k=2$ and 3 in Table 3.

Table 3: The constants c_{rj}.

k	r	j=0	j=1	j=2
	-1	3/2	-1/2	
2	0	1/2	1/2	
	1	-1/2	3/2	
	-1	11/6	-7/6	1/3
3	0	1/3	5/6	-1/6
	1	-1/6	5/6	1/3
	2	1/3	-7/6	11/6

The WENO reconstruction will take a convex combination of all $u_{i+\frac{1}{2}}^{(r)}$ and $u_{i-\frac{1}{2}}^{(r)}$ defined in (3.7), respectively, as the new approximations to $u(x_{i+\frac{1}{2}})$ and $u(x_{i-\frac{1}{2}})$ with $(2k-1)$th order accuracy:

$$u_{i+\frac{1}{2}}^{-} = \sum_{r=0}^{k-1} \omega_r u_{i+\frac{1}{2}}^{(r)}, \quad u_{i-\frac{1}{2}}^{+} = \sum_{r=0}^{k-1} \tilde{\omega}_r u_{i-\frac{1}{2}}^{(r)}, \qquad (3.9)$$

where the weights ω_r and $\tilde{\omega}_r$ are defined as

$$\omega_r = \frac{\alpha_r}{\sum_{s=0}^{k-1} \alpha_s}, \quad \tilde{\omega}_r = \frac{\tilde{\alpha}_r}{\sum_{s=0}^{k-1} \tilde{\alpha}_s}, \quad r=0,\cdots,k-1, \qquad (3.10)$$

with

$$\alpha_r = \frac{d_r}{(\epsilon+\beta_r)^2}, \quad \tilde{\alpha}_r = \frac{\tilde{d}_r}{(\epsilon+\beta_r)^2}. \qquad (3.11)$$

The values of d_r are given by

$$d_0 = \frac{2}{3}, \quad d_1 = \frac{1}{3}, \quad k=2;$$

$$d_0 = \frac{3}{10}, \quad d_1 = \frac{3}{5}, \quad d_2 = \frac{1}{10}, \quad k=3,$$

and $\tilde{d}_r = d_{k-1-r}$ from the symmetry. We choose the parameter $\epsilon = 10^{-6}$ in all the numerical tests. The so-called "smooth indicators", β_r, of the stencil $S_r(i)$ are given as follows:

$$\beta_0 = (u_{i+1} - u_i)^2, \quad \beta_1 = (u_i - u_{i-1})^2 \qquad (3.12)$$

for $k=2$, and

$$\beta_0 = \frac{13}{12}(u_i - 2u_{i+1} + u_{i+2})^2 + \frac{1}{4}(3u_i - 4u_{i+1} + u_{i+2})^2,$$
$$\beta_1 = \frac{13}{12}(u_{i-1} - 2u_i + u_{i+1})^2 + \frac{1}{4}(u_{i-1} - u_{i+1})^2, \qquad (3.13)$$
$$\beta_2 = \frac{13}{12}(u_i - 2u_{i-1} + u_{i-2})^2 + \frac{1}{4}(3u_i - 4u_{i-1} + u_{i-2})^2$$

for $k=3$.

Once the numerical fluxes $f_{i+\frac{1}{2}}$ are obtained by the WENO reconstruction procedures, the upwinding scheme is used in constructing the flux for stability. The Roe flux is applied,

$$\hat{f}_{i+\frac{1}{2}} = \begin{cases} u^-_{i+\frac{1}{2}}, & \text{if } a_{i+\frac{1}{2}} \geq 0, \\ u^+_{i+\frac{1}{2}}, & \text{if } a_{i+\frac{1}{2}} < 0, \end{cases} \qquad (3.14)$$

where $a_{i+\frac{1}{2}}$ is the Roe speed at $x_{i+\frac{1}{2}}$ defined as

$$a_{i+\frac{1}{2}} \equiv \frac{f(\theta_{i+1}) - f(\theta_i)}{\theta_{i+1} - \theta_i}. \qquad (3.15)$$

3.2 The time discretization using the TVD Runge-Kutta method

Now considering time discretization, we rewrite (3.5) as

$$\theta_t = L(\theta), \qquad (3.16)$$

where $L(\theta)$ is the WENO approximation to the derivative $-(\theta v)_x$ in the PDE (3.1). The optimal third order TVD Runge-Kutta method is employed:

$$\theta^{(1)} = \theta^n + \Delta t L(\theta^n),$$
$$\theta^{(2)} = \frac{3}{4}\theta^n + \frac{1}{4}\theta^{(1)} + \frac{1}{4}\Delta t L(\theta^{(1)}), \qquad (3.17)$$
$$\theta^{n+1} = \frac{1}{3}\theta^n + \frac{2}{3}\theta^{(2)} + \frac{2}{3}\Delta t L(\theta^{(2)}),$$

with CFL (Courant-Friedrichs-Levy) coefficient $c=1$.

Validation of the numerical method. We first test the numerical method using smooth solutions to check the order of the accuracy. The set-up of the test example is the following:

$$\theta_t + (v\theta)_x = 0,$$
$$v_{xx} + (\psi\theta)_x + (\sigma \ln(1-\theta))_x = 0,$$
$$\theta(0,t) = \theta(1,t), \quad v(0,t) = v(1,t), \qquad (3.18)$$
$$\theta_0(x) = \frac{1}{2} + \frac{1}{8}\cos(2\pi x),$$

where $\psi = 1.8$ and $\sigma = 1.0$. Since we do not know the exact solution of the system, we compare the computed results against the one computed from the finest grid which is $N = 1280$. The justification of such analysis can be found in [5].

Tables 4 and 5 list the grid refinement analysis against the solution computed from the finest grid. In the tables, the error ratio is defined as

$$\text{Ratio} = \frac{||U(2h) - U_*||}{||U(h) - U_*||},$$

where U stands for θ or v, U_* is the solution computed from the finest grid. Tables 4 and 5 show the ratios for θ and v at $t = 0.05$, respectively. The ratio approaches the number 5 indicating second order accuracy, while the number 3 would indicate first order accuracy (see the justification in [5]). We can see that the proposed method is second order accurate in both the L_1 and L_∞ norms at $t = 0.05$ for smooth solutions before any emerging shocks.

Table 4: Accuracy on θ in the System with $\theta_0(x) = \frac{1}{2} + \frac{1}{8}\cos(2\pi x)$.

n	L_∞ error	L_∞ ratio	L_1 error	L_1 ratio
10	7.98e-5	–	5.37e-5	–
20	2.73e-5	2.93	1.02e-5	5.26
40	6.48e-6	4.21	2.50e-6	4.08
80	1.65e-6	3.93	6.08e-7	4.12
160	4.11e-7	4.01	1.48e-7	4.12
320	9.82e-8	4.19	3.49e-8	4.24
640	1.96e-8	5.00	6.94e-9	5.02

Table 5: Accuracy on v in the System with $\theta_0(x) = \frac{1}{2} + \frac{1}{8}\cos(2\pi x)$.

n	L_∞ error	L_∞ ratio	L_1 error	L_1 ratio
10	2.65e-4	–	1.16e-4	–
20	6.97e-5	3.81	3.02e-5	3.84
40	1.74e-5	4.01	7.54e-6	4.00
80	4.37e-6	3.98	1.89e-6	4.00
160	1.08e-6	4.05	4.66e-7	4.05
320	2.57e-7	4.20	1.11e-7	4.20
640	5.13e-8	5.00	2.22e-8	5.00

When the initial data is piecewise constant, that is, with shock waves present, as in the standard approach, we measure the errors at some distance (0.1 in our test case) from the discontinuities. Tables 6 and 7 show the grid refinement results ($t = 0.05$) for θ and v with the following initial data:

$$\theta_0(x) = \begin{cases} 0.5, & \text{if } 0.3 \leq x \leq 0.7, \\ 0.1, & \text{if } x < 0.3 \text{ or } x > 0.7 . \end{cases}$$

Table 6: Accuracy on θ in the System with Discontinuous Initial Data.

n	L_∞ error	L_∞ ratio	L_1 error	L_1 ratio
10	5.28e-4	–	1.57e-4	–
20	2.65e-4	1.99	6.48e-5	2.42
40	1.32e-4	2.01	2.97e-5	2.18
80	6.65e-5	1.98	1.41e-5	2.10
160	3.32e-5	2.01	6.84e-6	2.06
320	1.56e-5	2.13	3.16e-6	2.16
640	5.66e-6	2.75	1.14e-6	2.77

Table 7: Accuracy on v in the System with Discontinuous Initial Data.

n	L_∞ error	L_∞ ratio	L_1 error	L_1 ratio
10	4.22e-3	–	1.26e-3	–
20	2.15e-3	1.96	5.91e-4	2.14
40	1.11e-3	1.94	2.91e-4	2.03
80	5.83e-4	1.91	1.49e-4	1.95
160	3.06e-4	1.91	7.74e-5	1.93
320	1.48e-4	2.07	3.71e-5	2.09
640	5.30e-5	2.79	1.33e-5	2.79

We obtained first order convergence for θ and v. This is due to the delta function singularity from $(\theta\psi)_x$ and $(\sigma\ln(1-\theta))_x$.

3.3 Applying the immersed interface method

To maintain accuracy for the velocity v near the discontinuities, we apply the immersed interface method (IIM) [6, 7]. The idea is simple. Initially, we know the locations of the discontinuities of θ, so we use the IIM to solve v to second order. Then from the computed velocity, we determine the new locations of the discontinuities and solve θ piece by piece accurately. The process then is repeated. We use Model 1 to illustrate the idea. The equation for v can be written as

$$\frac{\partial^2 v}{\partial x^2} = c_1\delta(x-x_1) + c_2\delta(x-x_2),$$

where $c_1 = -\psi + \sigma/(1-\theta)$ and $c_2 = -c_1$. The finite difference scheme from the IIM is

$$\frac{V_{j-1} - 2V_j + V_{j+1}}{(\Delta x)^2} = 0 + C_j, \tag{3.19}$$

where C_j is the correction term

$$C_j = \begin{cases} c_i \dfrac{h - |x - x_i|}{h^2}, & \text{if } |x - x_i| < h, \\ 0, & \text{otherwise,} \end{cases} \quad i = 1, 2.$$

The IIM gives more accurate results for both θ and v and eliminates non-physical oscillations (the Gibbs phenomenon). But in order to use this method, we need a prior knowledge of the shock locations.

4 Numerical examples

We take $L = 1$ for simplicity in this section. We have done a number of numerical experiments for different parameters. We want to know the long time behavior of the solution and whether θ (θ_u part) will grow and then stabilize. Our results indicate that θ in Model 1 grows faster compared with other models. In all cases presented here, we use dotted lines to represent the initial data, dash-dotted lines to represent the solution at the final time (often $T = 5$), and solid lines to represent the intermediate solution between initial and final time. The initial θ is piecewise constant with the discontinuities at $x_1 = 0.35$, $x_2 = 0.65$ with $\theta_l = 0.1$ and $\theta_u = 0.5$.

In Figs. 4 and 5, we show the computed results using the two different numerical methods with different parameters. By choosing the parameters according to our stability analysis, we obtained the desired results with θ in the middle part growing (the first plot in Figs. 4 and 5) or decaying (the lower bottom plot in Fig. 4). The solution will approach the steady states after some time.

From the computed results, we can conclude that the two methods, (1) the WENO and central finite difference scheme and (2) the IIM approach, give qualitatively the same results in the solution except at the discontinuities. The IIM approach eliminates the non-physical oscillations by enforcing the jump conditions in the finite difference scheme.

5 Conclusion

In this paper, we have studied a one-dimensional mixed model for cell modeling. The stability analysis has been conducted which gives the range of the parameters for the stability and their relations with parameters. Two different numerical methods were studied. The first one is the standard high order WENO scheme for the volume fraction of cells and fibers θ and a central finite difference scheme for the velocity v. In the second approach, we used the immersed interface method to enforce the jump conditions. The two methods give qualitatively the same results, but the second method using IIM eliminates non-physical oscillations with the knowledge of the locations of the shocks.
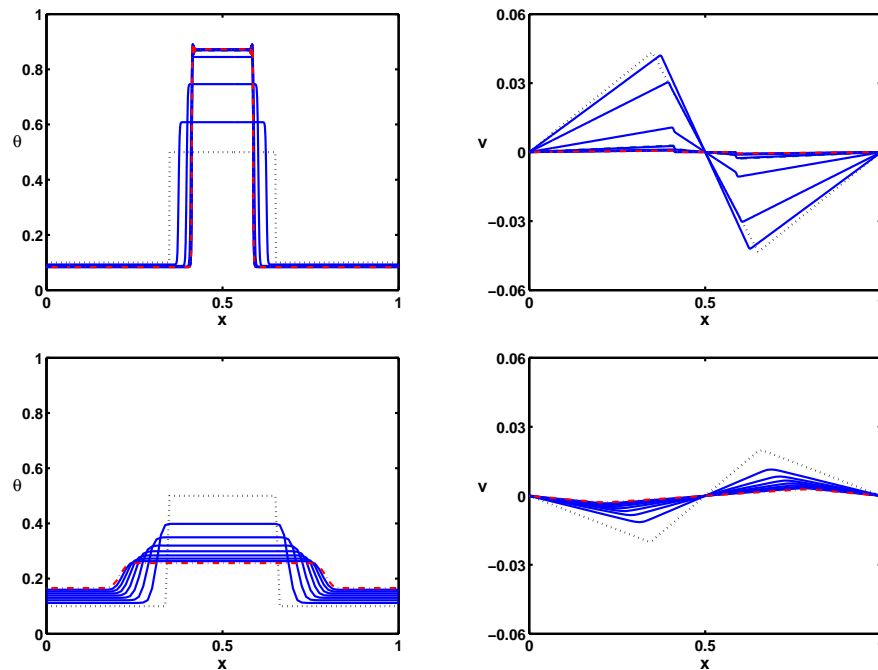
Figure 4: Computed solutions using the WENO scheme and central finite difference scheme with different parameters. The top two plots are computed with $\psi=2.5$, $\sigma=1$, and $N=640$. The solution θ grows in the middle. Some oscillations developed near the discontinuities. The bottom plots are computed with $\psi=1$, $\sigma=1$, and $N=80$. The solution θ decays and no oscillations occurred so we take a coarse grid. The final time is $T=5$ for the top plots while it is $T=20$ for the bottom ones since it takes longer time to reach the steady state solution.
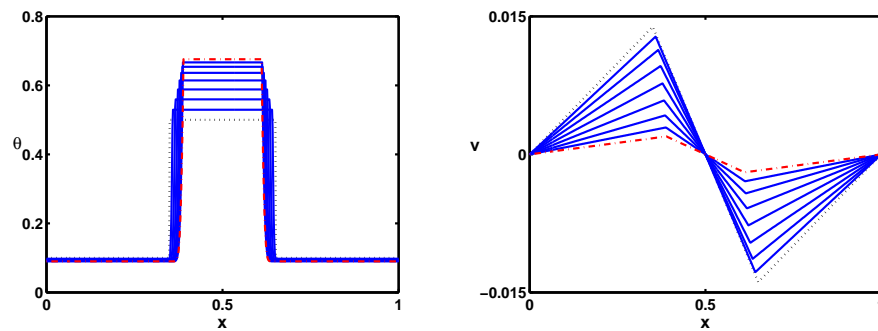

Figure 5: Computed solution using the IIM scheme. The results are computed with $\psi=1.8$, $\sigma=1$, and $N=640$. The final time is $T=5$. There are no oscillations in the computed solution.

Acknowledgments

References

[1] B. Cockburn, C. Johnson, C.-W. Shu, and E. Tadmor.   Lecture Notes in Mathematics - Advanced Numerical Approximation of Nonlinear Hyperbolic Equations. Springer, 1998.

[2] B. Costa, W. S. Don, D. Gottlieb and R. Sendersky   Two-dimensional multi-domain hybrid spectral-WENO methods for conservation laws.   Commun. Comput. Phys., 1 (2006), 548-574.

[3] M. Dembo and F. Harlow. Cell motion, constractile networks, and the physics of interpenetrating reactive flow. Biophysical Journal, 50 (1986), 109-121.

[4] G. Jiang and D. Peng. Weighted ENO schemes for Hamilton-Jacobi equations. SIAM J. Sci. Comput., 21(6) (2000), 2126-2143.

[5] Z. Li.   The Immersed Interface Method — A Numerical Approach for Partial Differential Equations with Interfaces. PhD thesis, University of Washington, 1994.

[6] Z. Li. An overview of the immersed interface method and its application. Taiwanese Journal of Mathematics, 7(1) (2003), 1-49.

[7] Z. Li and K. Ito. The Immersed Interface Method — Numerical Solutions of PDEs Involving Interfaces and Irregular Domains. SIAM Frontier Series in Applied Mathematics, FR33, 2006.

[8] S. R. Lubkin and T. Jackson. Multiphase mechanics of capsule formation in tumors.   J. Biomechanical Engineering-Transactions of the ASME, 124 (2002), 237-243.

[9] D. Manoussaki, S. R. Lubkin, R. B. Vernon, and J. D. Murray. A mechanical model for the formation of vascular networks in vitro. Acta Biotheoretica, 44 (1996), 271-282.

[10] Y. Xing and C.-W. Shu. A new approach of high order well-balanced finite volume WENO schemes and discontinuous Galerkin methods for a class of hyperbolic systems with source terms. Commun. Comput. Phys., 1 (2006), 100-134.